Journal of Applied Electrochemistry (2005) 35:1213–1223
DOI 10.1007/s10800-005-9032-8

Effect of composition on the surface and electrocatalytic properties of $Ti/IrO_x + RhO_x$ electrodes: H_2 evolution from acidic solution☆

L. POPA†, E. GUERRINI and S. TRASATTI*
*Department of Physical Chemistry and Electrochemistry, University of Milan, Via Venezian 21, 20133, Milan, Italy (*author for correspondence, e-mail: sergio.trasatti@unimi.it)*

Received 30 November 2004; accepted in revised form 11 April 2005

Key words: electrocatalysis, H_2 evolution, Ir oxide, mixed oxide electrodes, Rh oxide

Abstract

$IrO_x + RhO_x$ mixed oxide layers on a Ti support were prepared by thermal decomposition at 450 °C over the whole composition range. The temperature range 450–600 °C was explored for the composition 30 mol% RhO_x. Samples were characterized by means of SEM, XPS, cyclic voltammetry and polarization curves. Their electrocatalytic properties were tested for the H_2 evolution reaction. The following experimental parameters were scrutinized: voltammetric charge, Tafel slope, reaction order (H^+), electrical resistance of electrocatalysts. The electrocatalytic properties were evaluated at constant potential as a function of temperature as well as of composition. The electrode stability was assessed by comparing CV curves before and after groups of experiments. A reaction mechanism has been proposed. RhO_x is more active than IrO_x, its effect showing up for compositions >30 mol%.

1. Introduction

In view of the rising costs of fossil fuels and growing environmental pollution, the hydrogen economy is seen as a practical solution to the above problems. In this context, water electrolysis acquires a particular strategic role [1].

Precious metal oxides, such as RuO_x and IrO_x are very active for H_2 evolution, both in acidic as well as alkaline solutions [2–7]. Besides their intrinsic electrocatalytic properties, these oxides possess extended surface areas due to the thermal decomposition process used for their preparation [8]. Thus, geometric factors add to electronic factors to give very interesting performances as cathodes for H_2 evolution, also exhibiting good stability [9, 10] despite unfavourable thermodynamics conditions.

Recently, RhO_x has been investigated in this laboratory [11–14]. RhO_x exhibits better performances than RuO_x and IrO_x both in acids and in alkalis [3, 4]. In particular, mixtures of RuO_x and RhO_x show surface enrichment with RhO_x [14] so that electrodes with only 20% RhO_x exhibit already the behaviour of pure RhO_x. Since RhO_x is much more expensive than RuO_x, the advantage of using oxide mixtures is self-evident.

IrO_x is more active than RuO_x for H_2 evolution in acidic solutions [3, 4]. Therefore, it is of interest to investigate the properties of $IrO_x + RhO_x$ oxide mixtures to see whether synergic effects are operative with formation of more active cathodes than $RuO_x + RhO_x$ mixtures. The aim of this work has been to study H_2 evolution from acidic solutions on a series of $IrO_x + RhO_x$ mixed oxide electrodes prepared by thermal decomposition over the whole composition range.

2. Experimental

2.1. *Electrodes*

$Ti/IrO_x + RhO_x$ electrodes were prepared by thermal decomposition of $RhCl_3 \cdot 3H_2O$ (Fluka, 40% Rh) and of $IrCl_3 \cdot H_2O$ dissolved in aqueous HCl solution ($c = 0.1$ mol dm^{-3}; 10 w% HCl) to avoid hydrolysis. The solution was brushed onto a Ti support, the solvent evaporated at ca. 80–100 °C, and the sample calcined in a furnace in ambient atmosphere for 5 min at a temperature in the range 450–600 °C. The operation was repeated until the oxide loading was 2 mg cm^{-2}, with final calcination at the same temperature for 3 h.

Two series of electrodes were prepared. In a first series, the composition was varied in 10 mol% steps from 0 to 100% RhO_x, with calcination at 450 °C, two samples at each composition (total 22 electrodes). In a

☆In honour of Professor G. Kreysa on the occasion of his 60th birthday.
†On leave from Institute for Nuclear Research, Pitesti, Romania.

second series, the effect of the temperature of calcination (450–600°C at 50 °C steps) was studied for the composition 70% Ir + 30% Rh, two samples at each temperature (total 8 electrodes).

2.2. *Support*

Ti was used as a support in the form of platelets of $10\times10\times0.2$ mm size with a thin stem on one of the sides for the electrical connection. Before depositing the oxide, supports were first sandblasted with quartz powder, and then etched for 1 h in boiling 10 w% oxalic acid.

Samples were mounted in a Teflon holder as described elsewhere [15]. The apparent surface area exposed to the solution was 1 cm^2 on each of the two sides of the platelets. The electrical connection was made through a Cu wire welded to the upper part of the Ti stem (in the electrode holder) by means of a silver paste.

2.3. *Cells*

A four compartment cell was used throughout. Two Pt/Pt counterelectrodes faced the two sides of electrode samples. The reference electrode was connected to the main cell compartment via a Luggin capillary approaching the electrode from below. A gas inlet allowed the solution to be deaerated by means of purified N_2 (Sapio).

2.4. *Solutions*

Unless otherwise stated, solutions were 0.5 mol dm^{-3} H_2SO_4. They were prepared volumetrically with 95–97% H_2SO_4 (Fluka) and Millipore-MilliQ water. Solutions were deaerated for 1 h before commencing experiments. They were kept at 25 °C in a water thermostat, and under inert atmosphere during experiments.

2.5. *Potential scale*

Electrode potentials were measured and reported against a satd. calomel electrode (SCE).

2.6. *Electrochemical techniques*

Experiments were carried out using a Model 2053 AMEL potentiostat connected to a model 568 AMEL function generator. Cyclic voltammetry (CV) was usually operated at 20 mV s^{-1}. CV curves were recorded by means of Model 863 AMEL digital XY recorder.

Quasi-stationary potentiostatic curves were obtained by moving the electrode potential at 10 mV steps and reading the current after 1 min at each potential (forward scan). As the current reached about 100 mA, the direction of potential variation was reversed until the current became anodic (backward scan).

As reported by one of us in previous works [2, 4], RuO_2 and IrO_2 surfaces undergo hydration/activation with time or use. Precisely to avoid variable rates of gas evolution at a given overpotential, potentiostatic curves were repeated twice and reported current-potential values refer to the second run.

The order of reaction with respect to H^+ was determined by varying the acid concentration between 0.05 and 0.5 mol dm^{-3}. Two series of experiments were run. In one series the ionic strength was kept constant by means of Na_2SO_4 (constant 0.5 mol dm^{-3} total concentration). In another series, no Na_2SO_4 was added. Electrodes were first kept at −0.150 V (SCE) for 3 min, then at −0.200 V for 3 min, and at −0.330 V for additional 3 min, at the end of which current was read. Finally, the potential was stepped back to −0.200 V for 3 min and switched off. For each electrode only one reading was made in each solution.

2.7. *Non-electrochemical techniques*

The morphology of the oxide layers was observed on a Cambridge Stereoscan 150 scanning electron microscope (SEM).

The surface composition of the oxide layers was determined by means of X-ray photoelectron spectroscopy (XPS), using an M-probe (Surface Science Instruments, Mountain View, CA).

3. Results and discussion

After preparation, fresh samples were observed on a SEM and analyzed by XPS. Mounted as described elsewhere [15], electrodes were thus subject to the following experiments:

(1) Cyclic voltammetry in a limited potential range to obtain the 'electrochemical spectrum' of the surface (and the related surface charge). CV was repeated after each group of experiments.
(2) Quasi-stationary current-potential curves for the reaction of H_2 evolution (Tafel lines). This experiment was repeated twice not consecutively to check reproducibility.
(3) Determination of the reaction order with respect to H^+ in forward conditions of polarization.

3.1. *Surface morphology*

Figure 1 shows micrographs of samples of different composition. There is an evident change in morphology as the content of RhO_x increases. IrO_x appears much more microcrystalline and porous than RhO_x. Pure RhO_x looks like an amorphous matrix embedding micro-and nanocrystals. The particles appear to emerge from the matrix at 70 mol% RhO_x, while the matrix is no longer visible at <50 mol% RhO_x.

3.2. *Voltammetric curves*

Figure 2a shows a family of CV curves as a function of composition from pure IrO_x to pure RhO_x. At all

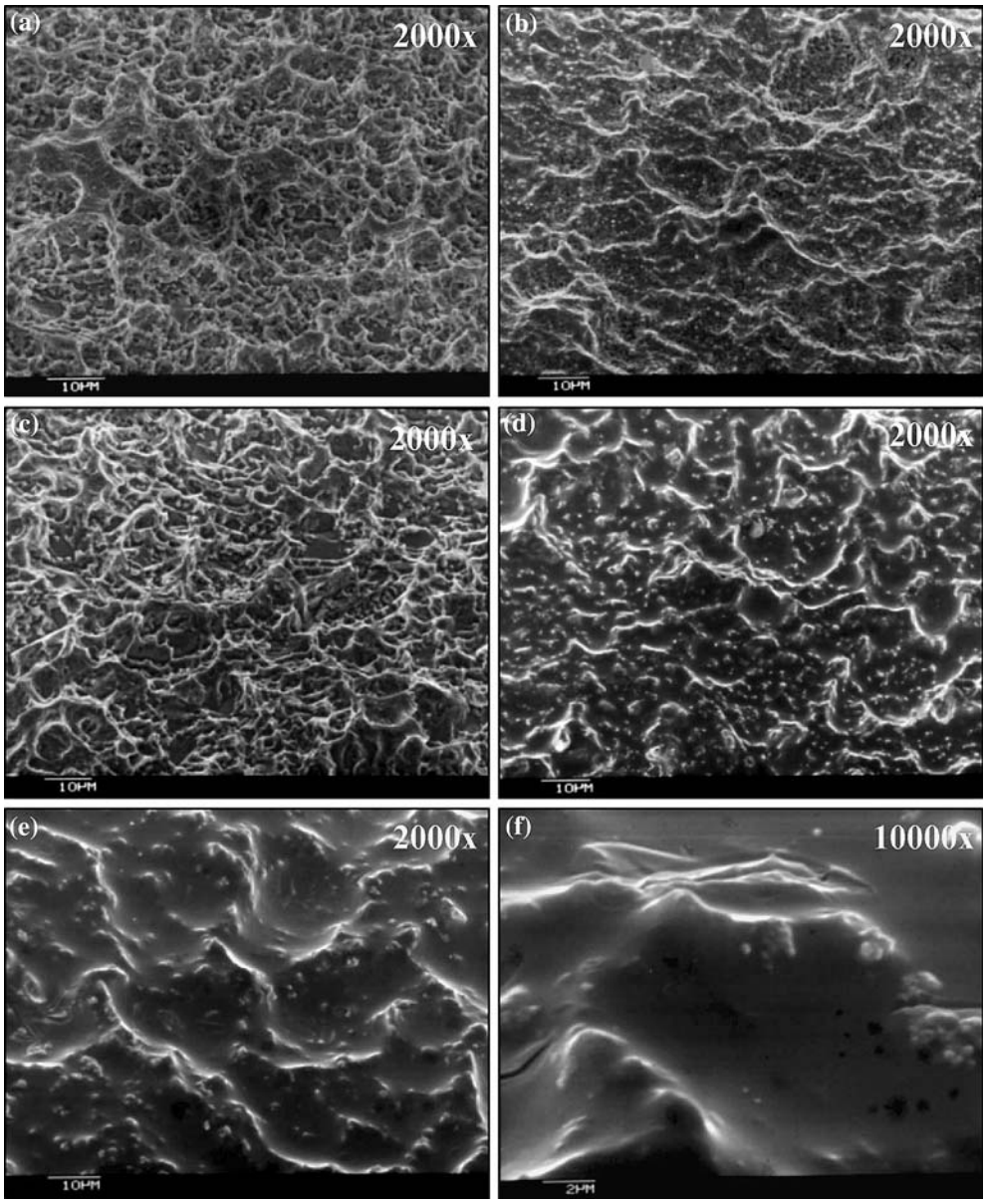

Fig. 1. SEM micrographs of fresh samples of $IrO_x + RhO_x$ at different contents of RhO_x. (a) 0; (b) 30; (c) 50; (d) 70; (e) 100; (f) 100 mol% RhO_x. Magnification: (a)–(e) ×2000; (f) ×10 000.

compositions the curves show a marked symmetry with respect to the *x*-axis, which points to good pseudocapacitive behaviour. Therefore, surface processes appear to be reversible.

The current density at a given potential is minimum for pure IrO_x and maximum for pure RhO_x. This anticipates an appreciable variation of the voltammetric (surface) charge with oxide composition.

The shape does not change dramatically across the composition range. Nevertheless, there are a few features which can be noted. While on the negative end of the potential range nothing appears to change as the composition varies, on the positive end it is evident that curves widen as the amount of RhO_x increases. At the same time, a small reversible hump shows up around 0.4 V (SCE) as the content of RhO_x becomes higher than 50 mol%. Such a small peak was observed also in previous works [13].

Figure 2b shows the effect of the calcination temperature on the CV curves of IrO_x (70%) + RhO_x (30%). The shape is closer to that of pure IrO_x and does not change with varying calcination temperature. This suggests that, from an electrochemical point of view, the chemical properties of the surface do not change. Nevertheless, a monotonic decrease of the current is observed with temperature, which points to a variation of the physical properties (e.g., morphology, surface area).

3.3. *Surface composition*

Samples were analyzed as received to test the same surface condition as that of fresh electrodes. Different samples, but prepared in the same batch, were used for XPS and CV experiments.

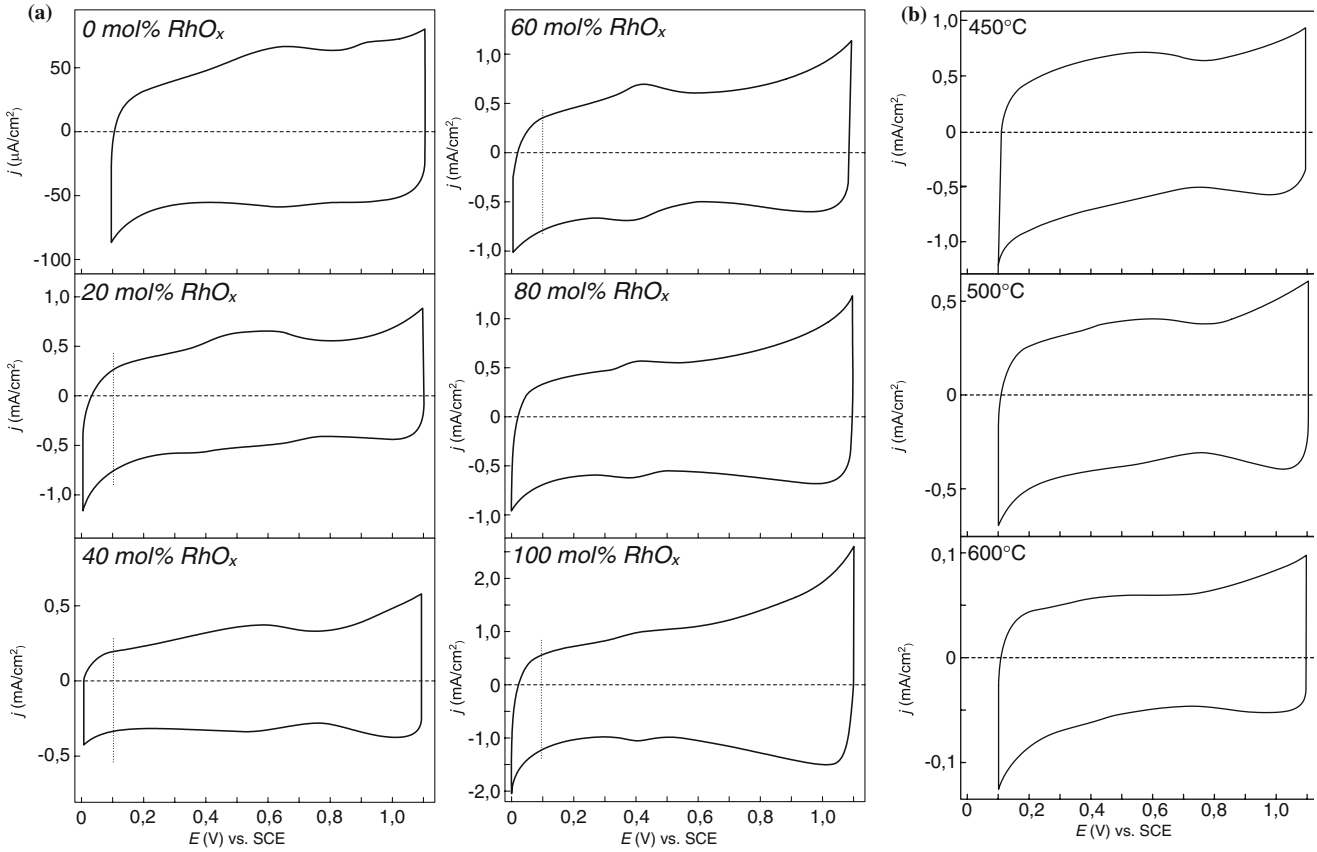

Fig. 2. (a) Cyclic voltammetric curves at 20 mV s^{-1} in 0.5 mol dm^{-3} H_2SO_4 solution of $IrO_x + RhO_x$ electrodes with different RhO_x contents (mol%), calcined at 450 °C. (b) Cyclic voltammetric curves at 20 mV s^{-1} in 0.5 mol dm^{-3} H_2SO_4 solution of 70 mol% $IrO_x + 30$ mol% RhO_x electrodes calcined at different temperatures.

Figure 3, empty circles, shows the XPS surface composition (mol% RhO_x) plotted vs. the nominal composition. Differently from the case of Ru + Rh mixed oxides [14], no appreciable enrichment of the surface with RhO_x is observed.

It has been shown in previous papers [16–18], that *in-situ* surface analysis of mixed oxide films can be carried out by CV, provided the two components exhibit separate features in the voltammetric curves. Figure 2a shows that current increases at positive potentials as the content of RhO_x increases, while the features on the left hand side of the curves do not change appreciably. Therefore, it is possible to take the ratio $R = j_1/j_{0.2}$, where $j_{0.2}$ and j_1 are the current density at $E = 0.2$ and 1.0 V, respectively, as representative of the content of RhO_x (R increases with increasing RhO_x content). The figure obtained can be normalized with the following operation:

$$\text{mol\% } RhO_x = \frac{(R_x - R_0)}{(R_1 - R_0)} \tag{1}$$

where the subscript of R refers to the mole fraction of RhO_x in the mixture. It is to be stressed that R does not depend on surface area since both $j_{0.2}$ and j_1 depend on the same surface area. Thus, surface area effects cancel out in the values of R. The CV data are reported in Figure 3 as asterisks. It is interesting that the CV surface analysis, although giving scattered data, is in satisfactory agreement with XPS data.

3.4. *Surface charge*

The voltammetric charge was determined by graphical integration of the voltammetric curves in the potential range 0.1–1.1 V (SCE). The integration included both cathodic and anodic charge, and the reported charge

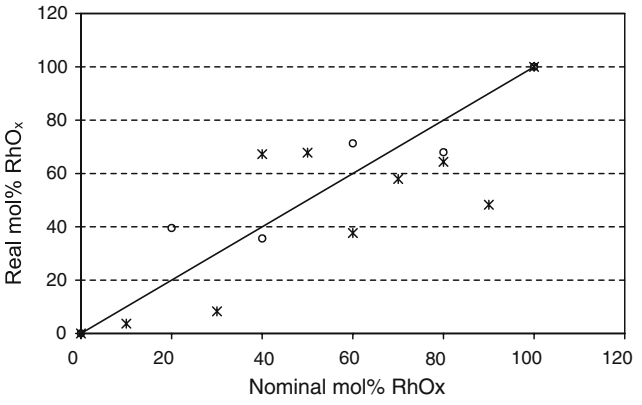

Fig. 3. Surface RhO_x content plotted against nominal RhO_x content of $IrO_x + RhO_x$ oxide layers. (○) XPS data; (*) Voltammetric data, from Equation 1 in the text. (-) Ideal straight line of unit slope (bisector).

density was obtained by dividing the total integrated charge by 2, the apparent surface area of the samples.

Figure 4a shows the voltammetric charge as a function of the nominal composition. The up-and-down behaviour of charge with composition is real since it was repeated with new electrodes prepared for the purpose. Interpretation is difficult. Tentatively, since phase separation gives rise to smaller particles than solid solutions, minimum and maximum could be related to compositions favouring intimate solid solution or not, respectively.

It could be tempting to correlate maxima and minima in Figure 4a with apparent maxima and minima in Figure 3. Closer inspection reveals that there is in fact no correlation. Since RhO_x exhibits a higher q^* than IrO_x, maxima in Figure 4a should correspond to surface enrichment with RhO_x which Figure 3 shows not to be the case. Nevertheless, the behaviour of XPS data could be non-monotonic. However, more specific and detailed XPS measurements would be necessary to clarify the issue.

A definite trend is that the charge, q^*, increases approximately in a linear fashion as the Rh content increases from 70 to 100 mol%. In the end, the charge of pure RhO_x is about one order of magnitude higher than that of pure IrO_x.

Figure 4b shows the effect of calcination temperature for samples with 30% RhO_x. This composition corresponds to a maximum in Figure 4a. As the calcination temperature increases, the surface charge decreases as expected due to crystallization and sintering effects.

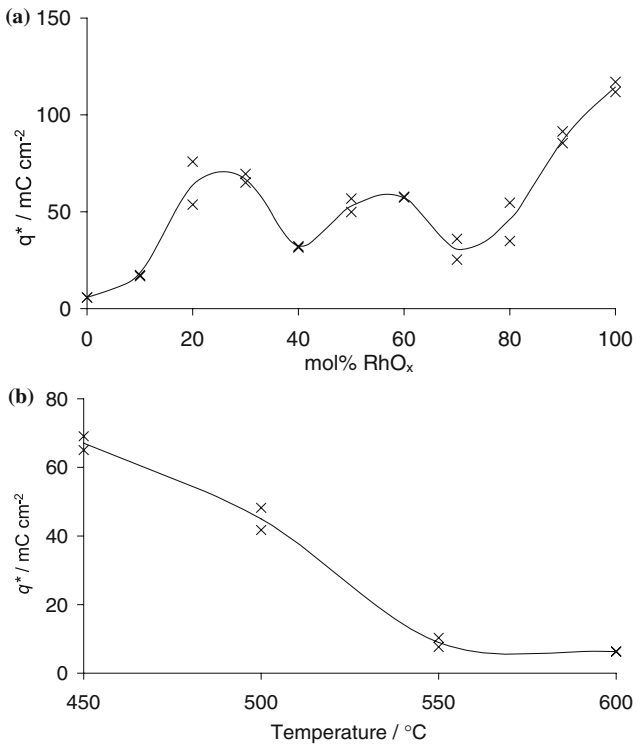

Fig. 4. (a) Apparent surface charge (q^*) as a function of nominal composition of $IrO_x + RhO_x$ oxide electrodes. q^* from integration of voltammetric curves (cf. Figure 2a). (b) Surface charge (q^*) as a function of calcination temperature of 70 mol% $IrO_x + 30$ mol% RhO_x electrodes. q^* from integration of voltammetric curves (cf. Figure 2b).

3.5. *Tafel lines*

Figure 5a shows a family of potentiostatic polarization curves for H_2 evolution on mixed oxide electrodes of various compositions, while Figure 5b shows similar curves for samples of the same composition prepared at different calcination temperatures. Tafel lines are non-linear in the high current density region. This can be due to uncompensated ohmic drops eventually in combination with a higher Tafel slope. It appears that with increasing IrO_x content a higher Tafel slope develops in the high current density range [2–4].

Tafel slopes were obtained from the Tafel lines in Figure 5a and b using two procedures [18].

(1) A straight line is drawn graphically from the linear part of the experimental curve in the low current range and extended to high currents. Here, deviations from the experimental points are determined (ΔE_{IR}) and plotted as a function of current (I). If a straight line is obtained (Ohm law), this indicates that deviations are only due to uncompensated ohmic drops, therefore, only one Tafel line is

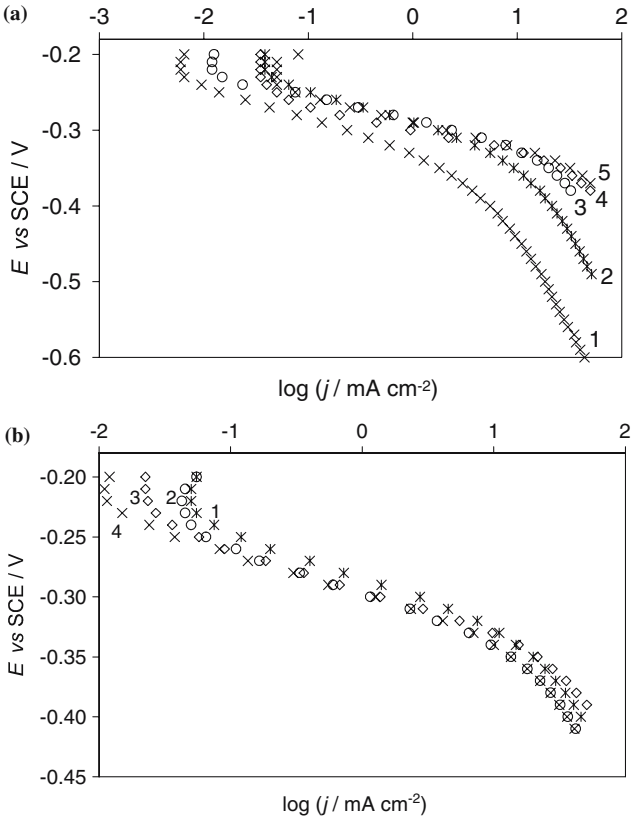

Fig. 5. (a) Family of polarization curves for H_2 evolution from 0.5 mol dm^{-3} H_2SO_4 solution on $IrO_x + RhO_x$ oxide electrodes of different compositions. (1) 0; (2) 20; (3) 50; (4) 80; (5) 100 mol% RhO_x; (b) Family of polarization curves for H_2 evolution from 0.5 mol dm^{-3} H_2SO_4 solution on 70 mol% $IrO_x + 30$ mol% RhO_x electrodes calcined at different temperatures. (1) 450; (2) 500; (3) 550; (4) 600 °C.

operating. The slope of the ΔE_{IR} vs. I straight line gives the uncompensated resistance between the electrode surface and the orifice of the Luggin capillary, as well as the resistance of the oxide overlayer – Figure 6a. If the ΔE_{IR} vs. I data give a curve, it means that two different Tafel lines are probably operating, or that the drawn Tafel line is inaccurate.

(2) A Tafel line in the presence of uncompensated ohmic drops can be written as:

$$E = a + b \ln I + \mathrm{IR} \tag{2}$$

Derivation with respect to I gives:

$$\mathrm{d}E/\mathrm{d}I = b/I + R \tag{3}$$

Thus, a plot $\Delta E/\Delta I$ (where ΔE and ΔI are the difference of two consecutive experimental points of potentiostatic curves) vs. $1/I$ (where I is the mean value between two consecutive values) gives a straight line whose slope is b (the customary Tafel slope value is obtained from $b\times$ 2.303) and whose intercept is R – Figure 6b. If more than one Tafel line exist, such a kind of plot will give a broken straight line whose slopes give the different Tafel slopes. The intercept R is that of the straight line at the highest currents.

3.6. *Tafel slopes*

Tafel lines were recorded twice at different times to investigate reproducibility. Tafel slopes were slightly higher in the first run for samples of high IrO_x content. This agrees with previous observations showing that the Tafel slope of 'aged' IrO_x is lower than for 'fresh' electrodes [19]. For this reason only second Tafel slopes are scrutinized here. The Tafel slopes reported in Figure 7 refer to the lower current density region.

Figure 7a shows the Tafel slope as a function of mixed oxide composition. The plot includes values obtained by the two procedures described in the previous section, for both forward and backward polarization. Two trends are recognizable: (1) the Tafel slope decreases slightly with Rh content from ca. 40 mV down to ca. 30 mV. Most of the decrease is observed between pure IrO_x and 20–30% RhO_x; (2) the Tafel slope for forward polarization is systematically slightly higher than for backward polarization. The difference is however probably not significant and might be related to the high concentration of atomic hydrogen adsorbed on the oxide surface during backward polarization.

The above observations are supported by the data at different temperatures, shown in Figure 7b where the Tafel slope spans from 30 to 40 mV depending on the direction of polarization. No appreciable change in Tafel slope is observed as the calcination temperature varies.

3.7. *Reaction mechanism*

Since Tafel slopes have standard values (from 30 to 40 mV), a reaction mechanism can be tentatively

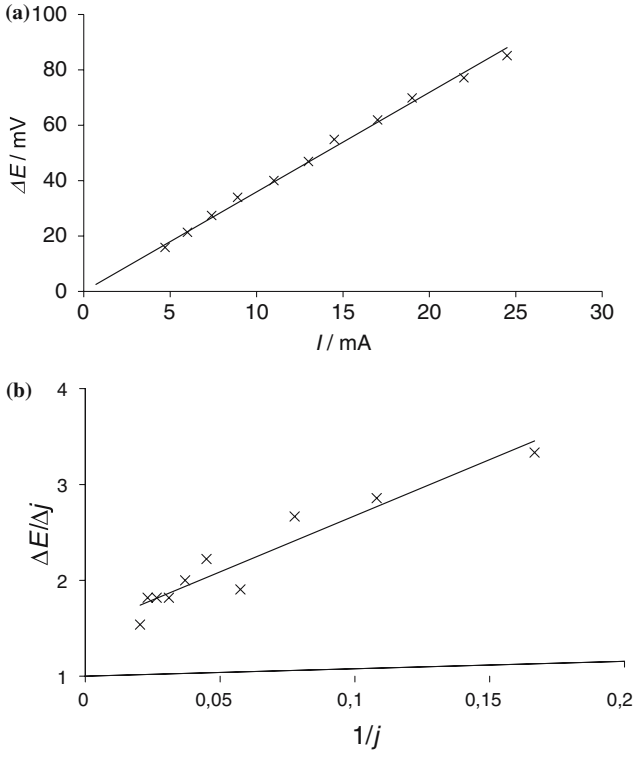

Fig. 6. (a) Typical plot of ΔE vs. I as described in Section 3.5. (1) Correlation coefficient 0.9954; (b) Typical plot of $\Delta E/\Delta I$ vs. $1/I$ as described in Section 3.5. (2). Correlation coefficient 0.9157.

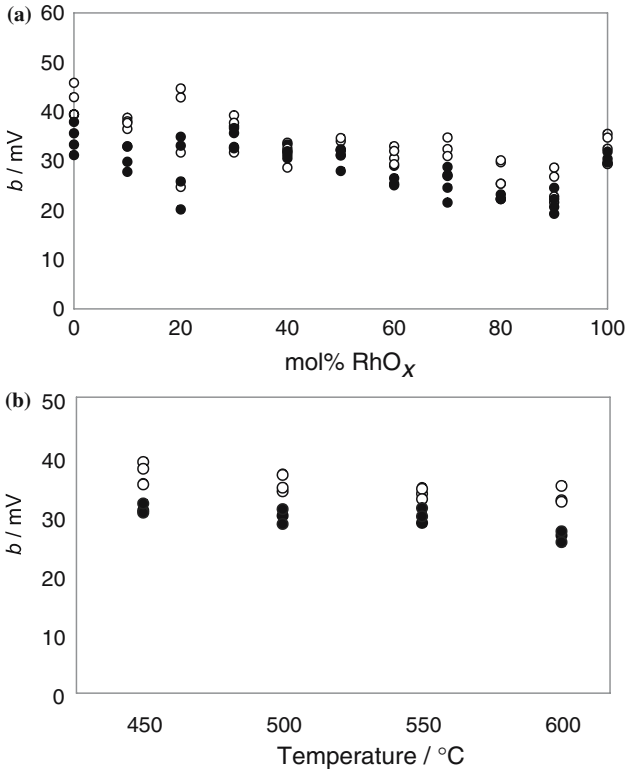

Fig. 7. Tafel slope for H_2 evolution from 0.5 mol dm^{-3} H_2SO_4 solution (a) on $IrO_x + RhO_x$ electrodes of different compositions and (b) on 70 mol% IrO_x + 30 mol% RhO_x calcined at different temperatures. (○) Forward and (●) backward potential scan.

proposed on the basis of this sole parameter. The Tafel slope varies from ca. 40 mV for pure IrO_x to ca. 30 mV for pure RhO_x. Thus, the mechanism is probably a classic one, comprising two of the following steps [2, 8]:

$$-MOH + H^+ + e \rightarrow -MOH_2 \quad (4)$$

$$-MOH_2 + H^+ + e \rightarrow -MOH + H_2 \quad (5a)$$

$$-MOH_2 + -MOH_2 + e \rightarrow 2\text{–}MOH + H_2 \quad (5b)$$

where –MOH is a surface active site, and steps (a) and (b) are alternative, in the sense that step (a) prevails on Ir sites, while step (b) prevails on Rh sites.

In the case of Ir-rich samples step (a) is predominantly the rds with a Tafel slope close to 40 mV; in the case of Rh-rich samples steps (b) is predominantly rate-determining with a Tafel slope close to 30 mV. The transition from the former to the latter mechanism is thought to be determined by a higher M–H bond strength on the surface of RhO_x. This will lead to an increasing surface coverage with the intermediate as Ir is replaced by Rh. The coverage will however, remain moderate altogether, since the Tafel slope remains low.

3.8. *Order of reaction*

The mechanism outlined above predicts an order of reaction with respect to H^+ equal to 2 in the case of both rds. This implies that the order of reaction should not vary either with composition or with calcination temperature.

The determination of the reaction order with respect to H^+ with oxide electrodes meets with additional problems. H^+ is a potential determining ion for oxide surfaces [20, 21], so that the determination of the reaction order at constant potential cannot be also at constant charge even if the ionic strength of the solution is kept constant. This problem has been previously discussed by one of us [22].

The reaction order was determined both at constant ionic strength and at variable ionic strength. Experiments showed that in both cases the measured reaction order differs from that calculated on the basis of the proposed mechanism. In particular, the reaction order is higher than 2 at constant ionic strength, and lower than 2 at variable ionic strength. This is shown in Figure 8 as a function of mixed oxide composition.

The effect of the potential determining ion is such as to decrease the expected reaction order giving a fractional reaction order. It has been calculated previously [22] that a reaction order of 1.5 should be observed as the Tafel slope is 40 mV. In other words the reaction order equals the transfer coefficient. Therefore, with a Tafel slope of 30 mV the reaction order with respect to H^+ should be 2. Figure 8 (curve 1) shows that the reaction order actually increases going from pure IrO_x ($b \approx 40$ mV) to pure RhO_x ($b \approx 30$ mV).

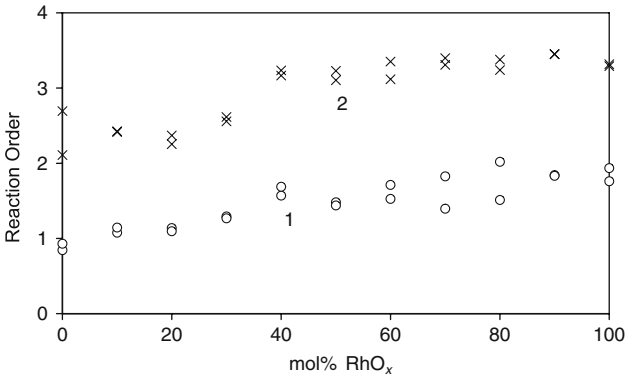

Fig. 8. Order of reaction with respect to H^+ for H_2 evolution from 0.5 mol dm^{-3} H_2SO_4 solution on $IrO_x + RhO_x$ electrodes of different compositions. (1) H_2SO_4 solutions at variable H^+ concentration; (2) $H_2SO_4 + Na_2SO_4$ solutions at variable H^+ concentration but constant ionic strength.

Reaction orders higher than the nominal values cannot be explained as due to the action of the potential determining ion, but effects related to ion adsorption cannot be neglected. IrO_x possesses a point of zero charge (pzc) close to 1 (i.e., very acidic) [20, 21]. Sulphate ions are strongly adsorbed on the IrO_x surface with an appreciable shift of the pzc to less acidic values [23].

The surface acid–base properties of RhO_x are not known, so that a value for the pzc is not available. On the basis of its 'electronegativity' [20, 21, 24] the pzc is expected to be higher than that of IrO_x. Thus, the RhO_x surface at the same pH should be more positively charged than that of IrO_x.

3.9. *Electrocatalytic properties*

In Figure 9a the effect of composition on the electrocatalytic properties is evaluated by plotting the observed reaction rate (current density) at a constant potential as a function of the RhO_x content. The higher activity of RhO_x with respect to IrO_x emerges clearly from the diagram, which is however divided into two parts. For RhO_x contents < 30 mol% the activity is constantly low whereas for RhO_x contents > 30 mol% it is constantly high. Thus, the major variation in activity takes place in the range 30–40 mol% RhO_x.

Figure 9b shows the effect of the calcination temperature at constant mixed oxide composition. Within the experimental uncertainty there appears a very slight increase of the electrocatalytic activity up to 550 °C, followed by an evident decrease at higher temperature.

Apparent reaction rates depend on both electronic and geometric factors. Allowance for the latter would give evidence to 'true' electronic (electrocatalytic) effects. Since the true surface is not directly known, it can be estimated in a relative way by means of the surface voltammetric charge which can be regarded as proportional to the surface concentration of active sites [8, 25].

Figure 10a and b show the reaction rate, normalized to the unit of surface charge (j/q^*), as a function of oxide

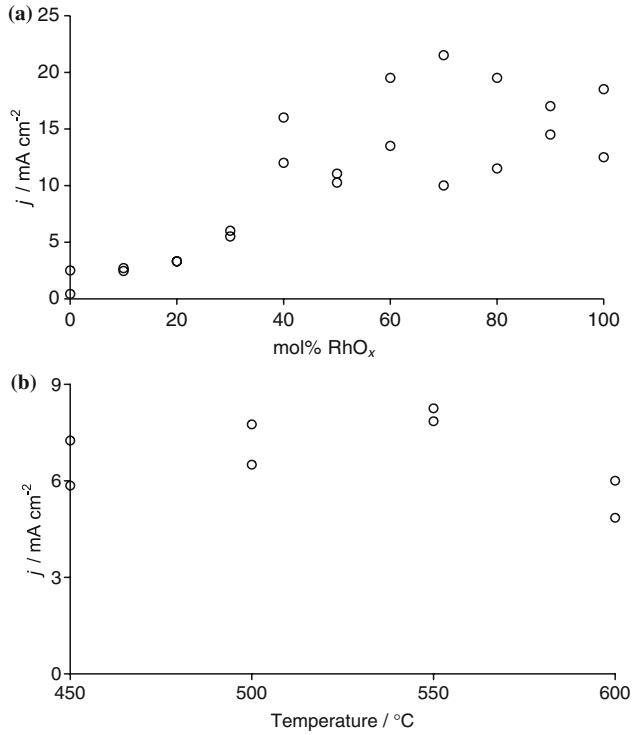

Fig. 9. (a) Apparent current density for H_2 evolution at −0.33 V (SCE) on $IrO_x + RhO_x$ electrodes of different compositions; (b) Apparent current density for H_2 evolution at −0.33 V (SCE) on 70 mol% IrO_x + 30 mol% RhO_x electrodes calcined at different temperatures.

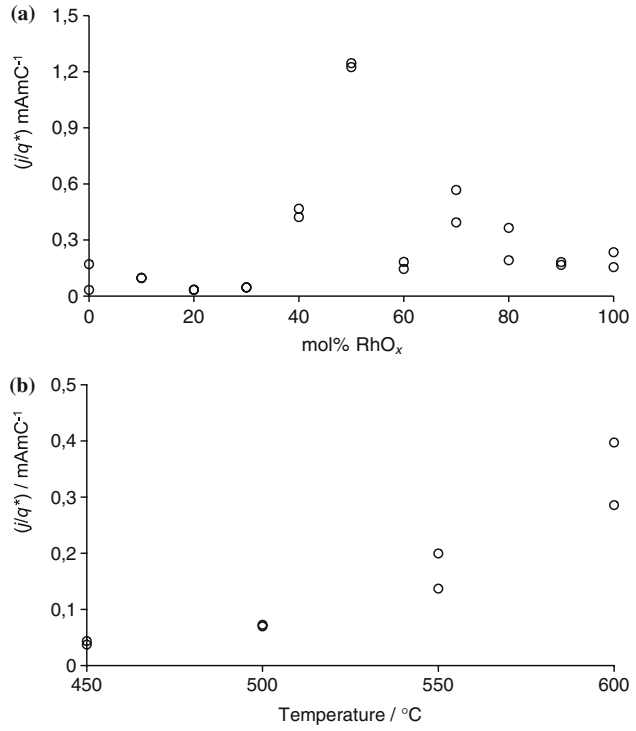

Fig. 10. (a) Normalized current density at −033 V (SCE) from Figure 9a as a function of electrode composition; (b) Normalized current density at −0.33 V (SCE) from Figure 9b as a function of calcination temperature.

composition and calcination temperature, respectively. In Figure 10a the normalized activity stays constant up to 30 mol% RhO_x then increases sharply to decrease at higher compositions than 50 mol% RhO_x. Thus, synergic effects appear to be operating at intermediate compositions. On the other hand, the 'true' electrocatalytic properties of pure RhO_x are comparable to those of IrO_x. In Figure 10b the 'true' electrocatalytic activity appears to increase with calcination temperature, an effect that has already been observed previously with RhO_x-based electrodes [12, 13].

3.10. *Electrode ohmic resistance*

The uncompensated ohmic resistance, determined by means of the approaches described in Section 3.5. can reveal barriers at the support/oxide interface related to the growth of insulating layers, e.g., TiO_2. In this evenience, experimental kinetic parameters might be distorted.

Figure 11a and b show the dependence of the electrode ohmic resistance on the mixed oxide composition, and on the calcination temperature at constant composition, respectively. In the latter case R amounts to about 0.5 ohm, which is typical for the electrolytic resistance between electrode surface and

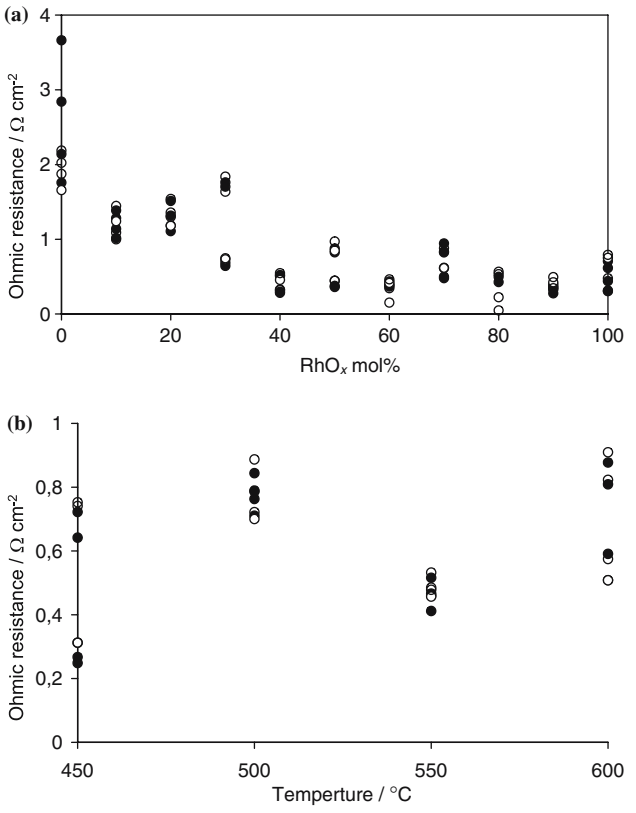

Fig. 11. (a) Uncompensated ohmic resistance in 0.5 mol dm^{-3} H_2SO_4 solution for $IrO_x + RhO_x$ electrodes of different compositions; (b) Uncompensated ohmic resistance in 0.5 mol dm^{-3} H_2SO_4 solution for 70 mol% IrO_x + 30 mol% RhO_x calcined at different temperatures. (○) Forward and (●) backward potential scan. Data from both procedures described in Section 3.5. are included.

Luggin capillary. This indicates that even at 600 °C the preparation of the oxide overlayer was accurate, so that no TiO_2 was allowed to grow on the support surface.

In Figure 11a, R maintains the same value as above from pure RhO_x up to about 30% RhO_x. As RhO_x decrease further, R increases up to ca. 2 ohm for pure IrO_x. The trend is clear and is unambiguously related to IrO_x. The explanation is difficult since IrO_x can in principle mix with TiO_2 being isomorphous, and in addition it is a metallic conductor [25]. However, Ir_2O_3 is known [26] to be poorly conductive. Since R is derived in conditions of H_2 evolution, a possible hypothesis is that the IrO_x layer is electrically degraded under H_2 evolution.

3.11. *Electrode stability*

It has been suggested by one of us [8, 25] that the state of the surface of an oxide electrode can be monitored by means of CV curves before and after a group of experiments. The parameters to scrutinize are the shape of the curve (electrochemical spectrum) and the voltammetric charge (proportional to the surface concentration of active site).

Figure 12b shows the evolution of the CV curves for two samples of the same composition (70% $IrO_x + 30\%$ RhO_x) calcined at two different temperatures, 450 and 600 °C, respectively. The shape and the size of the curves undergo some modification. After prolonged H_2 evolution the area of the curves

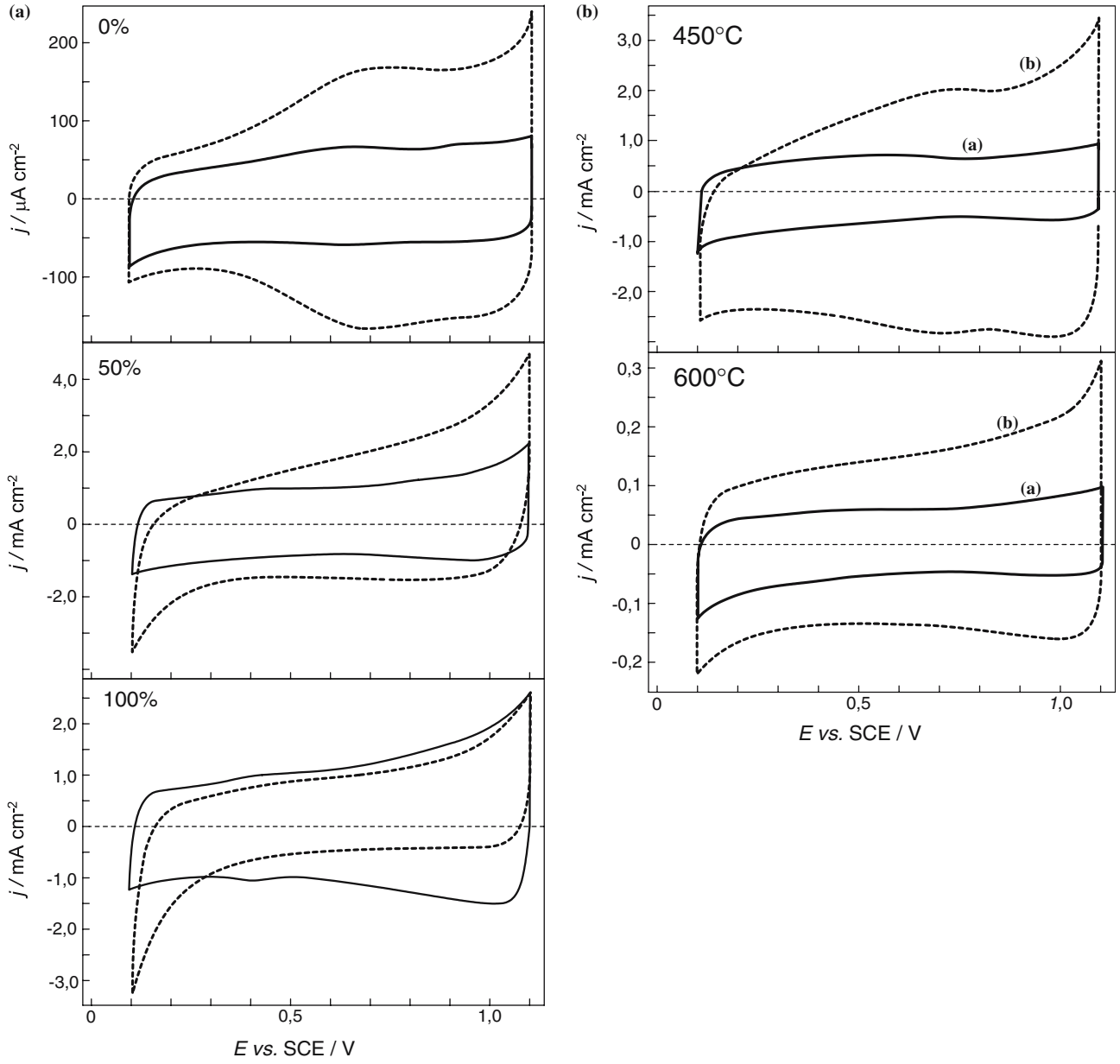

Fig. 12. (a) Evolution of voltammetric curves for $IrO_x + RhO_x$ electrodes of different composition (mol% RhO_x) (—) Fresh; (- - -) After intense H_2 evolution. (b) Evolution of voltammetric curves of $IrO_x + RhO_x$ electrodes calcined at different temperatures. (a) Fresh; (b) After intense H_2 evolution.

increases the more the higher the calcination temperature. In addition, a hump shows up around 0.7 V (SCE), the more the lower the calcination temperature.

The shape of the curves after H_2 evolution gets closer to that of IrO_x, which may indicate that the surface changes its composition. Nevertheless, the kinetic parameters (in particular, the Tafel slope) do not change with prolonged H_2 evolution. This implies that the reaction mechanism remains the same although the kinetic activity increases.

In the case of different mixed oxide compositions, Figure 12a illustrates the situation for three samples at 0, 50 and 100 mol% RhO_x, respectively. In the absence of RhO_x the features of IrO_x are exalted by prolonged H_2 evolution. In particular, the hump at about 0.7 V comes out definitely, while the whole CV curve 'swells.' This is in agreement with previous observations [27] and can be related to the spread of the solid/liquid interface to internal grain boundaries as a consequence of the hydrophilic induction of H^+ discharge.

As the RhO_x content increases, such an effect decreases so that the CV curves do not point unambiguously to a change of surface composition. In other words, there is evidence for 'cathodic' dissolution of one of the components. As the RhO_x content approaches 100%, however, on the negative end of the potential range the CV curve becomes markedly asymmetric with appearance of a decisively cathodic component. This is also in agreement with previous work. Pure RhO_x is reduced to metal under H_2 evolution and the CV curve evolves towards that of pure metal [13]. Thus, the incipient cathodic current is presumably related to the reduction of the surface oxide. Should the potential window be widened, the characteristic CV curve of Rh metal would appear. The presence of a second component decreases the trend of RhO_x to be reduced cathodically [14].

If the charge is scrutinized, some insight can be gained by comparing q^* for fresh electrodes with q^* for the same electrodes after a group of experiments. Figure 13a shows a plot for electrodes at different compositions before and after the determination of the first polarization curve. It is evident that, with the exception of two compositions, there is a general increase in q^* after H_2 evolution. If q^* after the first polarization curve is compared with q^* after the second polarization, Figure 13b shows unambiguously that electrode surfaces are satisfactorily stable. Therefore, H_2 evolution after an initial physical rearrangement of the interface does not produce further modifications. This is clear evidence for surface stability.

The effect of the calcination temperature suggests the same conclusions. Figure 14a shows that q^* increases of up to 100% after the first polarization curve, in quantitative agreement with previous observations. If q^* after the first PC is compared with q^* after the second polarization curve – Figure 14b – the charge is seen not to change appreciably. This indicates that these mixed

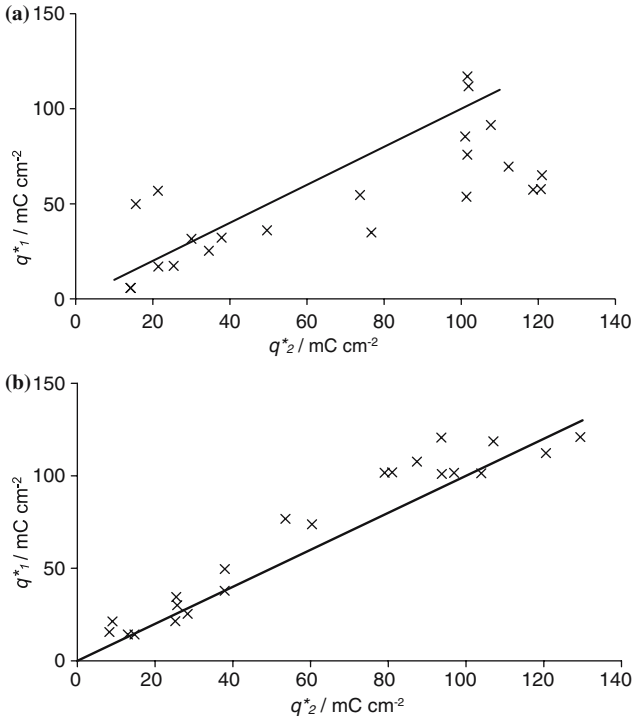

Fig. 13. (a) Voltammetric charge for fresh samples (q^*_1) plotted against voltammetric charge measured after the first determination of the Tafel slope (q^*_2) and (b) Voltammetric charge for samples after the first Tafel slope (q^*_1) plotted against voltammetric charge measured after the whole experimental study (q^*_2) for H_2 evolution on $IrO_x + RhO_x$ electrodes of different composition. (—) Straight line of unit slope.

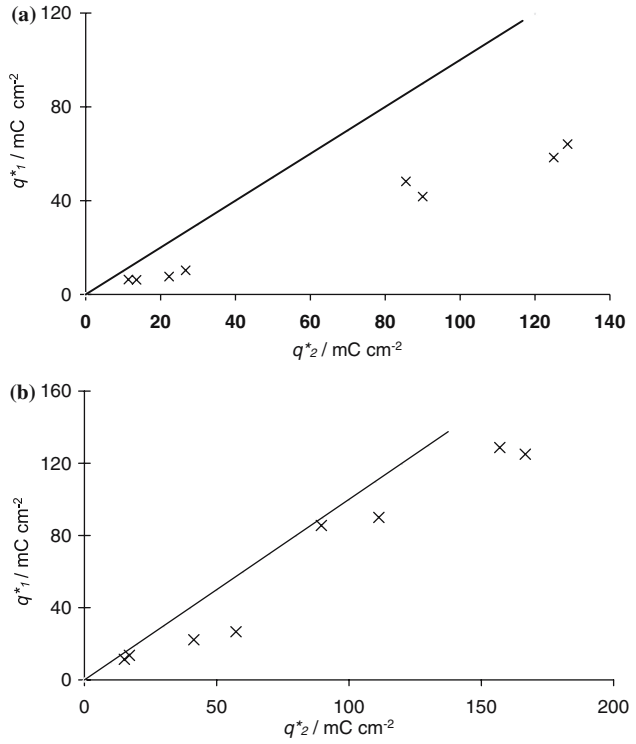

Fig. 14. (a) Same plot as in Figure 13a, for 70 mol% $IrO_x + 30$ mol% RhO_x electrodes calcined at different temperatures. (b) Same plot as in Figure 13b, for 70 mol% $IrO_x + 30$ mol% RhO_x electrodes calcined at different temperatures. (—) Straight line of unit slope.

oxide electrodes are substantially stable under intense H_2 evolution, at least in the time scale of these laboratory experiments. If the active layer were unstable with loss of material, q^* would be observed to decrease with use.

4. Conclusions

- The addition of RhO_x to IrO_x reduces the crystallinity of the oxide film as inferred from SEM observations.
- To a first approximation, the surface composition does not differ appreciably from the nominal composition.
- The surface composition can be monitored *in situ* by cyclic voltammetry.
- RhO_x is more active than IrO_x for H_2 evolution in acidic solution;
- The higher activity of RhO_x is mostly related to geometric factors;
- The 'true' electrocatalytic activity exhibits a maximum around 50 mol% RhO_x, thus providing evidence for moderate but definite synergic effects;
- The 'true' electrocatalytic activity of $IrO_x + RhO_x$ mixed oxide electrodes increases with increasing preparation temperature;
- $IrO_x + RhO_x$ oxide electrodes are stable under intense H_2 evolution in the conditions of the present laboratory experiments;
- The process of H_2 evolution proceeds with a low Tafel slope decreasing from ca. 40 to 30 mV with increasing RhO_x content;
- The evolution of the Tafel slope is very likely to be related to the adsorption strength of H_{ad} increasing from pure IrO_x to pure RhO_x.

Acknowledgements

Laurentiu Popa is grateful to the European Commission for a Marie Curie Fellowship during which this work was carried out. Thanks are due to the European Commission and MIUR (CoFin) for financial support to this work.

References

1. H. Wendt and G. Kreysa, *Electrochemical Engineering* (Springer-Verlag, Berlin, 1999).
2. S. Trasatti, *in* T.C. Wellington (Ed), 'Modern Chlor-Alkali Technology', (Elsevier Applied Science, Amsterdam, 1992), p. 281.
3. M. Kodintsev and S. Trasatti, *Electrochim. Acta* **39** (1994) 1803.
4. J.F.C. Boodts, G. Fregonara and S. Trasatti, *in* F. Hine, J.M. Fenton, B.V. Tilak and J.D. Lisius (Eds), 'Performance of Electrodes for Industrial Electrochemical Processes', Proc. Vol. 89–10, (The Electrochemical Society, Pennington, NJ, 1989), p. 135.
5. D. Miousse and A. Lasia, *J. New Mater. Electrochem. Syst.* **2** (1999) 71.
6. C. Chabanier, E. Irissou, D. Guay, J.F. Pelletier, M. Sutton and L.B. Lurio, *Electrochem. Solid State Lett.* **5** (2002) E40.
7. A. Cornell and D. Simonsson, *J. Electrochem. Soc.* **140** (1993) 3123.
8. S. Trasatti, *in* J. Lipkowski and P.N. Ross (Eds), 'The Electrochemistry of Novel Materials', (VCH Publishers Inc., 1994), p. 207.
9. M. Jaccaud, F. Leroux and J.C. Millet, *Mater. Chem. Phys.* **22** (1989) 105.
10. S. Trasatti, *Int. J. Hydrogen Energy* **20** (1995) 835.
11. Yu. E. Roginskaya, O.V. Morozova, G.I. Kaplan, R.R. Shifrina, M. Smirnov and S. Trasatti, *Electrochim. Acta* **38** (1993) 2435.
12. N. Kircheva, E. Guerrini and S. Trasatti, *Russian J. Electrochem.* **40** (2004) 1156.
13. M. Campari, A.C. Tavares and S. Trasatti, *Hem. Ind. (Chem. Ind. Beograd)* **56** (2002) 230.
14. E. Guerrini, M. Bregolato and S. Trasatti, *in* V. Birss, L. Burke, A.R. Hillman and R.S. Lillard (Eds), 'Surface Oxide Films', Proc. Vol. 2003–25, (The Electrochemical Society, Pennington, NJ, 2004), p. 1.
15. R. Garavaglia, C.M. Mari and S. Trasatti, *Surf. Technol.* **23** (1984) 41.
16. C. Angelinetta, S. Trasatti, Lj.D. Atanasoska and R.T. Atanasoski, *J. Electroanal. Chem.* **214** (1986) 535.
17. C.P. De Pauli and S. Trasatti, *J. Electroanal. Chem.* **396** (1995) 161.
18. N. Krstajić and S. Trasatti, *J. Electrochem. Soc.* **142** (1995) 2675.
19. H. Chen and S. Trasatti, *J. Indian Chem. Soc.* **70** (1993) 323.
20. A. Daghetti, G. Lodi and S. Trasatti, *Mater. Chem. Phys.* **8** (1983) 1.
21. S. Ardizzone and S. Trasatti, *Adv. Colloid Interface Sci.* **64** (1996) 173.
22. C. Angelinetta, M. Falciola and S. Trasatti, *J. Electroanal. Chem.* **205** (1986) 347.
23. S. Ardizzone, D. Lettieri and S. Trasatti, *J. Electroanal. Chem.* **146** (1983) 431.
24. M.A. Butler and D.S. Ginley, *J. Electrochem. Soc.* **125** (1978) 228.
25. S. Trasatti, *Electrochim. Acta* **36** (1991) 225.
26. L.D. Burke and D.P. Whelan, *J. Electroanal. Chem.* **124** (1981) 333.
27. S. Ardizzone, G. Fregonara and S. Trasatti, *J. Electroanal. Chem.* **266** (1989) 191.